Reduced Cell Attachment to Poly(2-hydroxyethyl methacrylate)-Coated Ventricular Catheters in Vitro

Brian W. Hanak[1,2,*], **Chia-Yun Hsieh**[3,*], **William Donaldson**[1], **Samuel R. Browd**[1,2], **Kenneth K.S. Lau**[3], and **William Shain**[1]

[1]Center for Integrative Brain Research, Seattle Children's Research Institute, Seattle, WA

[2]Department of Neurological Surgery, University of Washington, Seattle, WA

[3]Department of Chemical and Biological Engineering, Drexel University, Philadelphia, PA

Abstract

The majority of patients with hydrocephalus are dependent on ventriculoperitoneal shunts for diversion of excess cerebrospinal fluid. Unfortunately, these shunts are failure-prone and over half of all life-threatening pediatric failures are caused by obstruction of the ventricular catheter by the brain's resident immune cells, reactive microglia and astrocytes. Poly(2-hydroxyethyl methacrylate) (PHEMA) hydrogels are widely used for biomedical implants. The extreme hydrophilicity of PHEMA confers resistance to protein fouling, making it a strong candidate coating for ventricular catheters. With the advent of initiated chemical vapor deposition (iCVD), a solvent-free coating technology that creates a polymer in thin film form on a substrate surface by introducing gaseous reactant species into a vacuum reactor, it is now possible to apply uniform polymer coatings on complex three-dimensional substrate surfaces. iCVD was utilized to coat commercially available ventricular catheters with PHEMA. The chemical structure was confirmed on catheter surfaces using Fourier transform infrared spectroscopy (FTIR) and X-ray photoelectron spectroscopy (XPS). PHEMA coating morphology was characterized by scanning electron microscopy (SEM). Testing PHEMA-coated catheters against uncoated clinical-grade catheters in an in vitro hydrocephalus catheter bioreactor containing co-cultured astrocytes and microglia revealed significant reductions in cell attachment to PHEMA-coated catheters at both 17-day and 6-week time points.

Keywords

Catheter; Polymer; Cell Adhesion; Cell-material interactions; Shunt

Introduction

Hydrocephalus is a medical condition defined by the abnormal primary accumulation of cerebrospinal fluid (CSF) within the cerebral ventricles, which if untreated, produces

Correspondence: Dr. Brian W. Hanak, c/o Neuroscience Publications; University of Washington, Box 359924, 325 9th Ave, Seattle WA 98104, Tel.: (206) 685-3043; Fax: (206) 744-9942, publications@neurosurgery.washington.edu.
[*]Denotes co-first author status

increased intracranial pressures resulting in neurologic damage and even death.[1] For most patients with hydrocephalus the only way to manage their, generally lifelong, condition is to undergo surgical implantation of a CSF shunt, which diverts excess CSF from the cerebral ventricles to another body cavity. While CSF shunts have saved many lives since their advent in the 1950s,[2] modern shunt failure rates remain high, particularly in the pediatric patient population, with more than 40% of devices failing within two years of implantation. [3–7] Over half of these failures are caused by obstruction of the ventricular catheter (portion entering the cerebral ventricles) with cells and tissue.[7, 8] Specifically, studies using animal models[9–12] as well as analysis of catheters explanted from human patients[8, 13–16] have revealed that the resident innate immune cells of the central nervous system, astrocytes and microglia, appear to serve as the pathophysiologic lynchpin in the process of ventricular catheter obstruction by directly attaching to implanted catheter surfaces in large numbers, serving as an interface for the secondary binding of less reactive tissue types including choroid plexus to the catheter surface, and, presumably, through the recruitment of additional inflammatory cells to the site of an implanted foreign body via cytokine signaling.

Most modern, commercially available, ventricular catheters are poly(dimethyl)siloxane (PDMS)- or polyurethane (PU)-based blind-end tubes with CSF intake holes (approximately 500 μm diameter) with little science behind their design.[3, 17] Methods to improve shunt function have included both mechanical[18] and chemical modifications,[17] yet none have succeeded in reducing non-infectious occlusion rates in clinical practice. Chemically modified catheters, including antibiotic-impregnated (rifampin with either clindamycin or minocycline) and silver-coated catheters (combination of metallic silver and an insoluble silver salt), designed with an eye towards reducing shunt infection complications have become widely adopted in clinical practice in North America although studies have been mixed with respect to their efficacy.[19, 20] While a recent meta-analysis from Konstantelias et al. concluded that antibiotic-impregnated and silver-coated catheters appear to reduce the rates of early post-operative infections, their finding that the infections that do occur with these modified catheters tend to be associated with more virulent organisms, including Methicillin-resistant Staphylococcus aureus and gram-negative bacilli, warrants further study.[20] The only hydrogel surface-modified catheter that has been commercialized is the BioGlide ventricular catheter (Medtronic, Dublin, Ireland), which has a polyvinylpyrrolidone (PVP) coating that is designed to increase lubricity at time of surgical insertion. While the BioGlide catheter was not specifically marketed to inhibit cell attachment or subsequent obstruction, early in vitro studies of the PVP hydrogel coated catheters demonstrated reduced bacterial attachment.[21] Unfortunately, clinical studies in humans have failed to demonstrate reduced infection rates with the use of BioGlide catheters,[22] and one study even found statistically significant increases in infection rates.[23] The PVP hydrogel surface of BioGlide catheters, which is applied using traditional liquid phase synthesis techniques, is noted to have dewetting-related defects when imaged by scanning electron microscopy (SEM) in a dry state, and it is unknown if these cracks in the coating surface are completely eliminated by expansion of the hydrogel when the catheter is soaked in aqueous solution prior to surgical insertion.[24]

Over a half-century since they were first described by Wichterle and Lim,[25] poly(2-hydroxyethyl methacrylate) (PHEMA) hydrogels remain widely used for biomedical

applications, including drug delivery systems, as ophthalmic materials, and in biomedical implants given their proven biocompatibility and other desirable properties. Their hydrolytic stability and tunable porous structure allow various active agents to be carried and controllably released in relatively low dose.[26, 27] The resistance to protein fouling in addition to its extreme hydrophilicity has made PHEMA popular in contact lenses.[28, 29] In biomedical implants, PHEMA has served as a viable hydrogel scaffold for calcification and growth of bonelike composites.[30, 31] Furthermore, in PHEMA-coated neural prosthetic devices, local delivery of neurotrophins by lysine-conjugated PHEMA enhanced neuron survival and growth rate, potentially improving device performance in vivo.[32] PHEMA hydrogels have also been shown to weaken bacterial adhesion.[33] However, to our knowledge, only one previous publication has investigated the use of PHEMA in the context of CSF shunting, and this was a clinical study of eight pediatric hydrocephalus patients implanted with a novel ventriculo-subdural shunt made completely from PHEMA.[34] Unfortunately, given this study's focus on a rarely employed surgical technique, limited discussion of PHEMA shunt prototype fabrication methods, small sample size, and lack of a control group, this study does not provide insight into whether PHEMA hydrogel coatings have the potential to reduce rates of shunt failure from cellular obstruction. While PHEMA's hydrophilic nature makes it a strong candidate coating for ventricular catheters,[1, 2] the lack of prior attempts to fabricate PHEMA-coated ventricular catheters may simply reflect the historical challenge of applying a conformal polymeric coating to a complex three-dimensional structure. However, with the advent of the initiated chemical vapor deposition (iCVD) techniques in the early 2000s, which have made it possible to create highly uniform polymer coatings that conform to the topology of virtually any substrate surface, it is worth reconsidering whether altering the surface chemistry of CSF shunt catheters, even with well-studied hydrogels like PHEMA, might prove valuable in reducing the problem of cellular (astrocyte and microglia) attachement.[35]

iCVD is a unique solvent-free coating technology that directly creates a polymer in thin film form on a substrate surface by introducing gaseous reactant species into a vacuum reactor. Unlike conventional liquid-phase coating methods, the low-pressure iCVD environment and the lack of liquid surface tension or wettability effects enable highly conformal deposition on complex three-dimensional substrates at the micro- and nano-scale. A thorough discussion of the iCVD methodology has been detailed elsewhere.[36] Given the versatility in enabling organic synthesis and conformal coating, iCVD and iCVD polymers have been applied in a diverse range of applications, including photovoltaics,[37–39] superhydrophobicity,[40–42] icephobicity,[43] composites,[44] desalination,[45] and microfluidics. [46, 47] Among bio-related applications, the iCVD approach has been used in the fabrication of biosensors,[48, 49] controlled drug release applications,[50, 51] and to apply biopassive[52–54] and antimicrobial coatings.[55] In this work, we report a method for applying PHEMA to commercially available PDMS ventricular catheters using iCVD as well as preliminary evidence of reduced astrocyte and microglial attachment to PHEMA-coated catheters as compared to uncoated control catheters in an in vitro hydrocephalus catheter bioreactor. The iCVD approach enabled thinner 1–3 μm PHEMA coatings on catheters compared to conventional liquid processing methods, which for example produced much thicker 0.3–0.4 mm hydrogel coatings on catheters.[56] As a solvent-free process, iCVD avoid solvent issues,

such as solvent entrainment that may lead to catheter swelling and degradation. To our knowledge this represents the first published report to utilize iCVD technology to modify the surface chemistry of CSF shunt catheters with an eye towards reducing the primary mode of failure for these malfunction-prone, albeit life-saving, medical devices.

Experimental

Fabrication of PHEMA-Modified PDMS Ventricular Catheters

The catheters used in this study were standard, 32-hole (4 rows of 8 holes), PDMS ventricular catheters that are used clinically (Medtronic). The catheters were not impregnated with barium or antibiotics. The catheters were affixed to the cooled stage of the iCVD reactor without any pretreatment. For iCVD, 2-hydroxyethyl methacrylate monomer (HEMA) (97%, Sigma-Aldrich, St. Louis, MO) and di-tert-butyl peroxide initiator (TBPO) (99%, Acros Organics, Morris Plains, NJ) were used as received. Chromaloy (0.5 mm diameter, Goodfellow, Oakdale, PA) was employed as the heated filament material. For PHEMA synthesis, the iCVD conditions were 0.6, 0.18, and 0.2 standard cubic centimeters per minute (sccm) flows of HEMA, TBPO, and nitrogen (inert carrier gas), respectively, under a constant reaction pressure of 0.1 Torr. The filament temperature was maintained at 300 °C by resistive heating use a 600 W DC power supply (DLM 60-10, Sorensen, San Diego, CA) set at 1.4 A and 23.0 V. Through contact with an aluminium stage that is cooled to 25 °C with a 50:50 vol% water-ethylene glycol mixture in a recirculating chiller (RTE 7, Thermo Fisher Scientific, Waltham, MA), the catheter surface temperature was around 50 °C as measured by direct contact using a K-type thermocouple (Omega Engineering, Stamford, CT). To ensure more uniform coating around the samples and to minimize preferential coating on the top side of the catheters facing the filament array versus the underside that is in contact with the stage, iCVD was repeated under the same conditions after the samples were flipped over so the downside was up. Further details of the iCVD reactor system setup has been described.[44] It should be noted that no crosslinking agent has been used during iCVD PHEMA as the addition of the more hydrophobic crosslinker tends to reduce the hydrophilicity of PHEMA hydrogel critical for this study. Our prior studies have shown that uncrosslinked iCVD PHEMA deposited under the deposition conditions used here possess ultrahigh molecular weight that renders them practically insoluble in common solvents, including organic and aqueous media.[57]

Attenuated Total Reflectance Fourier Transform Infrared Spectroscopy

Attenuated total reflectance Fourier transform infrared (ATR-FTIR) spectra were taken on a Nicolet 6700 FTIR spectrometer (Thermo Scientific) using a zinc selenide crystal in the range of 500–4000 cm-1 at 4 cm-1 resolution and averaged over 32 scans. Air was used as the background for the pristine, uncoated PDMS catheter samples while a pristine PDMS catheter was used as the background for PHEMA-coated samples in order to isolate the characteristic peaks of PHEMA.

X-ray Photoelectron Spectroscopy

X-ray photoelectron spectroscopy (XPS) was performed on a PHI 5000 VersaProbe (Physical Electronics, Chanhassen, MN) with a monochromatic Al-Kα excitation source

(1486 eV) and charge compensation for the insulating samples. The X-ray beam diameter was 100 μm. High-resolution XPS spectra of C1s, O1s and Si2p core electrons were acquired using a 25 W beam of 100 μm diameter with 23.5 eV pass energy, 0.05 eV step size, 100 ms dwell time and averaged over 4 scans. The catheter samples were cut midway along their axial direction to enable analysis of both interior and exterior walls.

Scanning Electron Microscopy

Scanning electron microscopy (SEM) was conducted on a Zeiss Supra 50VP to elucidate surface morphology. The catheter samples were cut parallel to their axial direction to enable inspection of both interior and exterior surfaces. All SEM samples were sputtered with ≈10 nm Pt/Pd as a conductive layer to minimize charging during imaging. All images were taken at 2 kV to avoid damage to the polymer matrix. The magnification was set either at 5, 10, or 30 kX with a working distance of 2–3 mm.

Astrocyte Cell Culture

Procedures were approved by the Institutional Animal Care and Use Committee of Seattle Children's Research Institute in accordance with the National Institutes of Health Guide for Care and Use of Laboratory Animals. Primary astrocytes were collected from three-day old rat pups. Cortical hemispheres were removed and minced into 1-mm^3 pieces and suspended in calcium-free Hanks Balanced Salt Solution (Ca2+-free HBSS) (Invitrogen, Carlsbad, CA).

Following dissection and mincing, the Ca2+-free HBSS was removed and replaced by dissociation medium containing 0.25% trypsin-1X EDTA (Invitrogen) and incubated for 45 min at 37 °C with 5% CO2 in a 50 mL centrifuge tube. Fresh culture media was then added to quench the trypsin activity and the tube was centrifuged for 3 min at 1300 rpm to collect cells and tissue fragments (primary pellet). The resulting supernatant was collected, transferred into a new centrifuge tube, and centrifuged again to recover any cells that were not collected in the primary pellet. The primary pellet was cycled through a second dissociation and collection process to maximize cell recovery. The primary pellet and the supernatant pellets were then combined, resuspended, counted with a phase hemacytometer (Hausser Scientific, Horsham, PA), and plated on T-175 flasks (Invitrogen) at a density of 100,000 cells/mL, or approximately 1,000,000 cells/flask. Cultures were incubated at 37 °C with 5% CO2. Complete culture medium consisted of Dulbecco's Modified Eagle Medium (DMEM) supplemented with 4.5 g/L D-glucose, 584 mg/L L-glutamine, and 110 mg/L sodium pyruvate (Invitrogen), 5% fetal bovine serum (Invitrogen), 2% penicillin-streptomycin (Invitrogen), and 0.001% gentamicin (Sigma-Aldrich). When cells in primary cultures reached 80% confluence, cells not adherent to the culture flask were removed and the adherent astrocytes were dissociated from the flask surface using 0.25% trypsin-1X EDTA. After collecting the cells by centrifugation and resuspension in complete medium, cells were added to alginate scaffolds (see below) or were frozen using a CryoMed Controlled-Rate Freezer (Thermo Fisher Scientific) and stored in liquid N2 for future use. All cells used in these studies were passaged no more than three times. Astrocyte cultures were fed 3 times/week.

Microglial Cell Culture

A murine microglia cell line, "BV2," immortalized via the transfection of v-raf and v-myc oncogenes using a J2 retrovirus, was obtained directly from the Italian research group that created the cell line.[58] BV2 are widely used by researchers studying microglial function and, although BV2 cells may be more proliferative than primary microglia given the presence of oncogenes, they retain a very similar profile of gene expression when activated by exposure to lipopolysaccharide.[59] The BV2 microglial cell line was stored in liquid N2 and maintained in culture using the same methods described above for maintaining the primary astrocyte culture (same DMEM supplemented media, thrice weekly feeding, and 0.25% trypsin-1X EDTA dissociation methods).

In Vitro Cell Attachment Assay

Peptide-modified alginate was used to construct a 3D scaffold around shunt ventricular catheters. These scaffolds can support cell attachment and growth.[60–63] Alginate is a natural polysaccharide cross-linked in the presence of Ca2+ without the addition of cytotoxic agents.[61–63] Gel construction followed previously described methods.[61, 63, 64] A 1% (w/v) sodium alginate (Sigma-Aldrich) solution in 0.3 M NaCl and 0.1 M 2-(N-Morpholino)ethanesulfonic acid hydrate (MES buffer) was initially functionalized with an RGD peptide (GGGGRGDY, United Biosystems, Herndon, VA) to improve cell attachment and viability.[46, 62, 63] For standard carbodiimide crosslinking chemistry, the following reagents were added (in order) and incubated for 20 h at room temperature (RT): 8.22 g/L sulfo-N-hydroxysulfosuccinimide (Sigma-Aldrich), 16.44 g/L 1-ethyl-3-[3-dimethylaminopropyl]carbodiimide hydrochloride (Sigma-Aldrich), 0.3 g/L RGD peptide, and 10 g/L sodium alginate. The reaction was quenched by the addition of 13 g/L hydroxyl amine (Sigma-Aldrich). The functionalized alginate was then dialyzed using Snakeskin Dialysis Tubing (3.5K MWCO, Sigma-Aldrich). The initial dialysis solution contained 7.5 g NaCl/L Milli-Q® (EMD Millipore, Billerica, MA) deionized water (diH2O). Every 8 h the NaCl concentration was reduced by 1.25 g/L, with NaCl-free diH2O serving as the final solution. After dialysis, a charcoal filtration treatment was performed for 30 min. The sample was then lyophilized at 2000×10^{-3} mbar at -50 °C for five days. Prior to scaffold formation, a 5% stock of functionalized alginate was prepared using Ca2+-free HBSS.

Ventricular catheter testing chambers were assembled using an open polycarbonate base with an inlet and outlet ports, a glass coverslip bottom secured with silicone glue, and a loosely-fitted polycarbonate top. The PHEMA-coated and uncoated control catheters were mounted within the test chambers and the catheter tips were secured to the glass coverslip bottom with a small dab of silicone glue. The chambers containing the catheters to be tested were then sterilized by means of super critical CO2 sterilization (Nova2200, NovaSterilis, Lansing, NY).

Following sterilization, the in vitro ventricular catheter test chambers were fitted with sterile polycarbonate "dams" which served as a mold for subsequent alginate polymerization around the catheter. In order to seal the spaces between the dam, catheter, and chamber floor, 4% (w/v) low-melt agarose solution (Sigma-Aldrich) in sterile Milli-Q diH2O was added to the chamber on either side of the dam. Next, to promote alginate attachment to the chamber

surfaces, 0.01% poly-L-lysine (PLL) (Sigma-Aldrich) was added to the portion of the chamber contained by the dam for 2 h at 37 °C and then washed in a bath of Milli-Q diH2O for 5 min.

In preparation for alginate hydrogel scaffold construction, cultured primary astrocytes and BV2 microglia were dissociated with 0.25% trypsin-1X EDTA, counted using the phase hemacytometer, and resuspended in Ca2+-free HBSS at a concentration of 6,000,000 astrocytes and 1,500,000 microglia per 477 μL. Alginate hydrogels/scaffolds were then constructed by mixing a sterile stock solution of 6% (w/v) calcium carbonate (Sigma-Aldrich), Ca2+-free HBSS containing astrocytes and microglia, D-(+)-gluconic acid delta-lactone (GDL) (Sigma-Aldrich), and the functionalized, dialyzed, and lyophilized alginate prepared as a 5% (w/v) stock (see above). The final alginate concentration was 1.5% (w/v) using a 0.54 Ca:COOH molar ratio following previously published methods.[6] To make the scaffold, the 6% CaCO3 solution was vortexed to evenly distribute the CaCO3 in the supersaturated solution. 57 μL of CaCO3 was pipetted into a 250 mg alginate aliquot and mixed, followed by the addition of 477 μL of Ca2+-free HBSS containing astrocytes and microglia. Working quickly, 50 μL of 214 mg/mL GDL was added to the mixture and stirred. The total mixture was then pipetted into the potential space of the polycarbonate dam (within the ventricular catheter testing chamber) and incubated in a cell culture incubator (37°C and 5% CO2) for 90 min to enable crosslinking. Following this initial 90-min incubation period, the dam and surrounding agarose were carefully removed and the chamber was filled with supplemented DMEM cell culture media.

Culture media was replaced 3 times weekly. At the 17-day or 6-week cell culture time point, the catheters were fixed with 4% paraformaldehyde, applied at RT for 1 h. Following fixation the catheters were washed with three rapid rises of HEPES-Buffered Hanks Solution (HBHS) containing sodium azide (90 mg/L; pH 7.4) and stored in buffer at 4°C until processed for imaging.[65]

Immunohistochemistry

The ventricular catheters maintained in HBHS containing sodium azide were removed from storage at 4°C and incubated in 5 mg/mL of sodium borohydride in HBHS for 30 min at RT to reduce postfixation-crosslinking autofluorescence. Next, the catheters were incubated in 0.2% Triton-X-100 (Sigma-Aldrich) in HBHS for 30 min at RT for cell membrane permeation to permit antibody penetration to intracellular sites. Catheters were then incubated in Image-iT FX signal enhancer (Invitrogen) for 30 min at RT to prevent nonspecific labeling.

Catheters were labeled with 1:800 monoclonal rat anti-glial fibrillary acidic protein (GFAP), an astrocyte marker (Invitrogen) and 1:800 monoclonal rabbit anti-Ionized calcium-binding adapter molecule 1, a microglia marker (Iba1, Wako Pure Chemical Industries, Osaka, Japan) for 24 h at RT. Subsequently, 1:200 goat anti-rat Alexa Fluor 488 (Invitrogen) and 1:200 goat anti-rabbit Alexa Flour 647 (Invitrogen) conjugated secondary antibodies were applied for 24 h at RT. Additionally, at the time of secondary antibody application catheters were stained with 1:1000 Hoescht (Sigma-Aldrich) for identification of cell nuclei and

rhodamine phalloidin (1:150, Invitrogen) for visualization of cytoskeletal actin (cell morphology visualization).

After 24h in secondary antibodies and Hoescht, the catheters were washed 4 times over 30 min with HBHS containing sodium azide and 0.5% TWEEN 20 (Sigma-Aldrich). Lastly, the ventricular catheters were mounted with Fluoromount-G (SouthernBiotech, Birmingham, AL) in custom polycarbonate imaging chambers, which allowed for the application of cover slips to both sides of the chamber (for ease of imaging of CSF intake holes oriented on opposite sides of the catheter).

Catheter Imaging

Three-dimensional, multispectral spinning disk confocal microscopy was utilized to image ventricular catheters (IX81 Inverted Microscope, motorized X-Y-Z stage, broad-spectrum light source, charged-coupled camera, Olympus, Tokyo, Japan). $800 \times 800 \times 502$ μm confocal images were acquired in and around catheter CSF intake holes (10× objective; 209 optical Z-sections with a 2.4-μm step size). For each catheter analyzed, one half of the 32 CSF intake holes were systematically imaged (n=16). The exposure times and gain settings were kept constant on all images acquired.

Quantification of Cell Attachment

Differences in cellular attachment to ventricular catheters were quantified using MetaMorph Microscopy Automation & Image Analysis Software (Molecular Devices, Sunnyvale, CA). All images were processed in a standardized fashion. First, to reduce background autofluorescence and image noise, the images were processed with a median filter (nonlinear digital filtering technique; filter width: 2 pixels; filter height: 2 pixels; subsample ratio: 1) followed by background subtraction technique ("flatten background"; object size: 25 pixels). Next, the Z-stack images (containing 209 optical sections) were collapsed into a single image using a maximum projection function. The resulting single plane maximum projection image was then thresholded using an inclusive threshold state. Since variability in background and noise were still present in some samples, thresholds were selected to produce a visually consistent background. After obtaining an appropriate threshold, a circular region (standardized size for all samples) was loaded onto the maximum projection image so that the entire CSF intake hole was contained within the region. Using the established threshold, integrated fluorescence intensity was then calculated within the standardized circular region. All integrated fluorescence intensity values are presented in millions.

Statistics

Integrated fluorescence intensity values are reported as the mean ± standard error of the mean and compared using a Mann-Whitney U test. Statistical analysis was performed using the Statistical Package for the Social Sciences 20.0 (SPSS) (IBM, Armonk, NY). Statistical significance is defined as $p < 0.05$.

RESULTS AND DISCUSSION

In order to apply a conformal PHEMA coating to clinically-used PDMS ventricular catheters, the iCVD protocol, in brief, involves the delivery of monomer and initiator vapor flows into the iCVD chamber that is operated under a mild vacuum (≈0.1–10 Torr); the initiator is thermally activated selectively by an array of resistively heated filaments (≈300–400 °C); the monomer and activated initiator diffuse to the surface of the sample sitting on a cooled stage (≈25 °C); subsequent monomer adsorption leads to surface polymerization at the activated initiator sites, resulting in the growth of a polymer film that conforms to the topology of the substrate surface (Figure 1(a)). The reaction mechanism for the iCVD polymerization of HEMA[65] follows conventional free radical polymerization,[64] which, as shown in Figure 1(b) involves the thermal decomposition of a free radical initiator (e.g. peroxide) and the chain linkage of monomer units through opening of the vinyl bonds.

Following iCVD coating of ventricular catheters, the chemical structure of PHEMA was confirmed by FTIR and XPS spectroscopy. Figure 2 shows the ATR-FTIR spectra of the PDMS catheters before and after PHEMA coating. From the spectrum of pristine (uncoated) PDMS, two major peaks appearing at 1007 and 786 cm-1 are attributed to Si–O–Si and Si–$(CH_3)_2$ stretching on the PDMS structure, respectively. Smaller peaks located at 1258 cm-1 and 2963 cm-1 corresponding to the deformation and stretching of CH_3, respectively. After iCVD coating, the spectrum (with the PDMS background removed) shows a peak centered around 3434 cm-1 corresponding to the broad absorption band of OH and a peak at 1726 cm-1 associated with C=O. These chemical groups are only found on PHMEA (see Figure 1) and suggest that iCVD PHEMA film was deposited on the PDMS catheters. These peaks along with other PHEMA characteristic peaks, including CO stretching (1300–1200 cm-1), CH bending (1500–1350 cm-1) and CH stretching (3050–2800 cm-1), were similar to iCVD PHEMA FTIR spectra published previously.[66] The region below 1100 cm-1 shows residual and negative absorptions related to artifacts from subtraction of the PDMS background.

To more quantitatively define the chemical structure of iCVD PHEMA coated on the catheters, high resolution XPS spectra were acquired as shown in Figure 3. From Figures 3(a)-(c), the C1s, O1s and Si2p3/2 peaks of PDMS located at 284.7, 532.0 and 101.6 eV, respectively, correspond to peaks of the PDMS polymer.[35] For Si2p, there is an additional Si2p1/2 peak located at 102.3 eV, which is due to spin orbit splitting that has the expected binding energy split and 1:2 intensity ratio relative to the Si2p3/2 peak. For C1s and O1s, there are peaks located at 284.2 and 531.6 eV, respectively, which can be attributed to adventitious adsorbed impurities from exposure to the atmosphere that were present on the catheter surfaces since no sample cleaning or pretreatment was carried out. From the fitted high resolution spectra, after accounting for elemental sensitivity factors, the estimated atomic ratio between carbon, oxygen and silicon of uncoated PDMS is 2.1:1.0:1.0, which is close to the theoretical ratio of 2:1:1 for stoichiometric PDMS. The XPS peaks and their assignments are summarized in Table 1.

After depositing iCVD PHEMA on the PDMS catheters, as shown in Fig. 3(D)-(F), only peaks associated with the PHEMA are visible. Given that XPS is a surface-sensitive technique, probing only about 10 nm of the top surface, the much thicker PHEMA coating

essentially blocks the underlying PDMS from being probed, and so the Si2p peak from the PDMS has disappeared completely. The C1s and O1s peaks correspond to that of PHEMA only, as seen by the fitted peaks and their corresponding assignments that are also provided in Table 1. The estimated carbon to oxygen ratio of iCVD PHEMA is 2.5:1.0, which is close to the theoretical ratio for stoichiometric PHEMA.[67] The quantitative XPS data coupled with the qualitative FTIR results demonstrate that iCVD PHEMA with the expected PHEMA chemistry has been formed. The much lower amount of carbon (and no oxygen) impurities observed on the PHEMA surface compared to the uncoated PDMS surface is due to the clean iCVD environment during PHEMA synthesis as well as to careful post-iCVD storage of samples in vacuum-sealed containers prior to XPS analysis.

The morphology of uncoated and iCVD PHEMA-coated PDMS catheters as revealed by SEM are shown in Fig. 4. The pristine PDMS catheter surface is smooth and void of any large surface features based on the top and side views as shown in Fig. 4(A,B). After iCVD PHEMA deposition, the surface morphology became rougher as seen in the top views in Fig. 4(C,E) and there is a clear demarcation of the PHEMA coating from the underlying PDMS substrate in the side views in Fig. 4(D,F). The PHEMA coating appears to fully cover the catheter surface with no noticeable defects such as pinholes or cracks. But visually there are differences in the PHEMA coating on the exterior catheter wall in Fig. 4(C,D) compared to that on the interior wall in Fig. 4(E,F). Clearly, the PHEMA coating is much thicker on the exterior wall (>3 μm) compared to that on the interior wall (1–2 μm) when the coating side views on the exterior and interior walls are compared. This is understandable given there is greater and more facile access to reactants on the exposed surface during the iCVD process. From the top views, it appears that there are greater surface undulations of the PHEMA coating on the interior wall. Typically, larger and rougher surfaces features are associated with a nucleation-limited process in chemical vapor deposition.[68, 69] In iCVD, the delivery of activated initiator species to the interior surface could be hindered as these species need to travel through the CSF-intake holes (diameter: ≈500 μm). Since the activated initiator species serve as the nucleation agents for polymer growth, their lower concentration in the catheter interior could give rise to fewer nucleation events and result in larger, rougher polymer structures. The lower nucleation density also supports the slower polymerization kinetics that yielded the thinner polymer coatings. In contrast, the diffusion of activated initiator to the exposed exterior surface is practically unhindered and nucleation density could be much higher, leading to the smaller surface undulations and thicker coatings observed.

To further investigate the PHEMA coating morphology along the catheter, several points in the vicinity of the intake holes and closed end have been analyzed by SEM as shown in Fig. 5. SEM images were taken of the exterior and interior catheter walls at various locations as well as of the intake hole sidewall for the 8 holes in a given row. Consistent with observations in Fig. 4, for all locations probed, the PHEMA has a rougher surface texture with larger surface features on the interior wall compared to the exterior wall that is attributed to the higher nucleation density. In further support of this claim, the surface roughness and feature sizes of PHEMA on the intake hole sidewalls fall between that of the smoother exterior wall coating and the rougher interior wall coating. Since the activated initiator has to pass through the intake holes to reach the inside of the catheter tube, the

concentration of these species at the intake hole sidewall will most likely be at an intermediate level between the more accessible exterior and less accessible interior. In terms of morphological variations with different positions along the catheter, there does not appear to be any significant change except perhaps near the blind end where the accumulation of activated initiator species around the interior wall might see an increased nucleation density and correspondingly a surface that is not as rough. The largely uniform coating morphology at different locations indicates the conformal nature and spatially well-distributed reaction medium of the iCVD process. PHEMA-coated and uncoated control catheters were tested in an in vitro hydrocephalus catheter bioreactor containing co-cultured astrocytes and microglia within an alginate hydrogel scaffold simulating brain parenchyma in order to determine if the PHEMA coating conferred a resistance to cellular attachment.[70] Cellular attachment was measured through analysis of integrated fluorescence intensity values obtained from three-dimensional confocal microscopy imaging of rhodamine-phalloidin (F-actin probe conjugated to the red-orange fluorescent dye, tetramethylrhodamine) stained cells attached at the surfaces of catheter CSF intake holes. CSF intake holes were the focus of this analysis given prior study of obstructed ventricular catheters operatively removed from children in shunt failure, which demonstrated that CSF intake holes serve as niduses for astrocyte and microglia attachment.[8]

We found significant reductions in cell attachment to PHEMA-coated catheters at both 17-day and 6-week cell culture time points. At the 17-day time point, the control and PHEMA-coated catheter CSF intake holes had mean integrated fluorescence intensity values of 8.88 ± 1.97 (n=16) and 1.98 ± 0.46 (n=16), respectively, thus demonstrating highly significant reduction of cell attachment with the PHEMA coating ($p = 0.0027$). At the 6-week time point, the control and PHEMA-coated catheter CSF intake holes had mean integrated fluorescence intensity values of 3.88 ± 0.49 (n = 32) and 1.51 ± 0.22 (n = 32), respectively, thus demonstrating highly significant reduction of cell attachment with the PHEMA coating ($p=0.00038$). Figure 6 demonstrates representative images of the actin stain for half of the control and PHEMA-coated catheter holes imaged at the 17-day time point alongside the calculated integrated fluorescence intensity values for those same holes. In addition to quantitative differences in integrated fluorescence intensity values, the nature of cell attachment to the control versus PHEMA-coated catheters appears qualitatively distinct. In particular, while cells form clusters that extend beyond the PDMS surface of the control catheter CSF intake holes, such clustering is essentially absent on PHEMA-coated catheters. Instead, cells bound to the CSF intake hole surfaces of the PHEMA-coated catheters form a, generally sparse, monolayer.

Conclusions

This study demonstrates the feasibility of using iCVD to apply polymer coatings to CSF shunt ventricular catheters. The decreased astrocyte and microglia cell attachment to PHEMA-coated catheters tested in an in vitro hydrocephalus catheter bioreactor suggests that this approach could prove valuable for producing more failure-resistant next generation ventricular catheters.

The qualitative difference in the nature of cell attachment to the CSF intake holes of control versus PHEMA-coated catheters – with cells clustering and extending off the CSF intake hole sidewalls in the control catheters versus forming a sparse monolayer along the hole sidewalls of the PHEMA-coated catheters – may prove clinically significant as cell clustering within the CSF intake holes is more likely to result in reductions of CSF flow and ultimately catheter obstruction. It is possible that the rough surface texture of the PHEMA coating allowed for single cell attachment between the hydrogel gobbets. If this is the case, the lack of cell clustering on the PHEMA catheters may be because the hydrogel gobbets between the attached cells prevented contact/interaction between neighboring cells. It is also possible that the cells seen on the CSF intake hole sidewalls of the PHEMA-coated catheters were more weakly attached than their counterparts on the control catheter hole sidewalls and therefore could not support the attachment of additional cells not in direct contact with the catheter surface. While this preliminary study demonstrates feasibility of the general technique of iCVD coating of ventricular catheters, further work will certainly be needed in order to optimize the system for the targeted function. Operating on the hypothesis that a smoother surface is better at mitigating cell binding,[70–72] future efforts to generate smoother coatings would be focused on enhancing the nucleation density and availability of activated initiator species used in the iCVD protocol. This could be achieved by increasing the filament temperature, raising the vapor concentration of initiator flow, and/or reducing the substrate temperature. Another potential approach for obtaining smoother coatings would be to perform a post-deposition thermal anneal of the polymer coating near or above its glass transition ($\approx$75–90 °C) to induce some amount of polymer flow and redistribution. It is also possible that coating smoothness might also be improved if there is better adhesion and compatibility of the hydrophilic PHEMA polymer with the underlying hydrophobic PDMS substrate. By carrying out air or oxygen plasma surface pretreatment of the catheters prior to iCVD, the catheter surface might favor enhanced surface nucleation, polymer growth, and consequently better integration of the polymer with the substrate. Although PHEMA has been selected in this study, primarily due to its widespread adoption as a viable biomaterial, other polymer hydrogels like poly(ethylene oxide) (PEO) and poly(vinylpyrrolidone) (PVP), which have been successfully synthesized by iCVD,[53, 73] might also be good candidates to explore.

Acknowledgments

References

1. McAllister JP 2nd, Williams MA, Walker ML, Kestle JR, Relkin NR, Anderson AM, et al. An update on research priorities in hydrocephalus: overview of the third National Institutes of Health-

sponsored symposium "Opportunities for Hydrocephalus Research: Pathways to Better Outcomes". J Neurosurg. 2015; 123(6):1427–38. [PubMed: 26090833]

2. Aschoff A, Kremer P, Hashemi B, Kunze S. The scientific history of hydrocephalus and its treatment. Neurosurg Rev. 1999; 22(2–3):67–93. discussion 4–5. [PubMed: 10547004]

3. Lutz BR, Venkataraman P, Browd SR. New and improved ways to treat hydrocephalus: Pursuit of a smart shunt. Surg Neurol Int. 2013; 4(Suppl 1):S38–50. [PubMed: 23653889]

4. Browd SR, Gottfried ON, Ragel BT, Kestle JR. Failure of cerebrospinal fluid shunts: part II: overdrainage, loculation, and abdominal complications. Pediatr Neurol. 2006; 34(3):171–6. [PubMed: 16504785]

5. Scott RM, Madsen JR. Shunt technology: contemporary concepts and prospects. Clin Neurosurg. 2003; 50:256–67. [PubMed: 14677444]

6. Pollack IF, Albright AL, Adelson PD. A randomized, controlled study of a programmable shunt valve versus a conventional valve for patients with hydrocephalus. Hakim-Medos Investigator Group. Neurosurgery. 1999; 45(6):1399–408. discussion 408–11. [PubMed: 10598708]

7. Kestle J, Drake J, Milner R, Sainte-Rose C, Cinalli G, Boop F, et al. Long-term follow-up data from the Shunt Design Trial. Pediatr Neurosurg. 2000; 33(5):230–6. [PubMed: 11155058]

8. Hanak BW, Ross EF, Harris CA, Browd SR, Shain W. Toward a better understanding of the cellular basis for cerebrospinal fluid shunt obstruction: report on the construction of a bank of explanted hydrocephalus devices. J Neurosurg Pediatr. 2016; 18(2):213–23. [PubMed: 27035548]

9. Bruni JE, Del Bigio MR. Reaction of periventricular tissue in the rat fourth ventricle to chronically placed shunt tubing implants. Neurosurgery. 1986; 19(3):337–45. [PubMed: 3762881]

10. Del Bigio MR, Bruni JE. Reaction of rabbit lateral periventricular tissue to shunt tubing implants. J Neurosurg. 1986; 64(6):932–40. [PubMed: 3701444]

11. Del Bigio MR, Fedoroff S. Short-term response of brain tissue to cerebrospinal fluid shunts in vivo and in vitro. J Biomed Mater Res. 1992; 26(8):979–87. [PubMed: 1429759]

12. Del Bigio MR. Biological reactions to cerebrospinal fluid shunt devices: a review of the cellular pathology. Neurosurgery. 1998; 42(2):319–25. discussion 25–6. [PubMed: 9482182]

13. Sarkiss CA, Sarkar R, Yong W, Lazareff JA. Time dependent pattern of cellular characteristics causing ventriculoperitoneal shunt failure in children. Clin Neurol Neurosurg. 2014; 127:30–2. [PubMed: 25459240]

14. Hanak BW, Bonow RH, Harris CA, Browd SR. Cerebrospinal Fluid Shunting Complications in Children. Pediatr Neurosurg. 2017

15. Sekhar LN, Moossy J, Guthkelch AN. Malfunctioning ventriculoperitoneal shunts. Clinical and pathological features. J Neurosurg. 1982; 56(3):411–6. [PubMed: 7057239]

16. Blegvad C, Skjolding AD, Broholm H, Laursen H, Juhler M. Pathophysiology of shunt dysfunction in shunt treated hydrocephalus. Acta Neurochir (Wien). 2013; 155(9):1763–72. [PubMed: 23645322]

17. Harris CA, Resau JH, Hudson EA, West RA, Moon C, Black AD, et al. Reduction of protein adsorption and macrophage and astrocyte adhesion on ventricular catheters by polyethylene glycol and N-acetyl-L-cysteine. J Biomed Mater Res A. 2011; 98(3):425–33. [PubMed: 21630435]

18. Harris CA, McAllister JP 2nd. Does drainage hole size influence adhesion on ventricular catheters? Childs Nerv Syst. 2011; 27(8):1221–32. [PubMed: 21476036]

19. Kestle JR, Holubkov R, Douglas Cochrane D, Kulkarni AV, Limbrick DD Jr, Luerssen TG, et al. A new Hydrocephalus Clinical Research Network protocol to reduce cerebrospinal fluid shunt infection. J Neurosurg Pediatr. 2016; 17(4):391–6. [PubMed: 26684763]

20. Konstantelias AA, Vardakas KZ, Polyzos KA, Tansarli GS, Falagas ME. Antimicrobial-impregnated and -coated shunt catheters for prevention of infections in patients with hydrocephalus: a systematic review and meta-analysis. J Neurosurg. 2015; 122(5):1096–112. [PubMed: 25768831]

21. Cagavi F, Akalan N, Celik H, Gur D, Guciz B. Effect of hydrophilic coating on microorganism colonization in silicone tubing. Acta Neurochir (Wien). 2004; 146(6):603–10. discussion 9–10. [PubMed: 15168229]

22. Kaufmann AM, Lye T, Redekop G, Brevner A, Hamilton M, Kozey M, et al. Infection rates in standard vs. hydrogel coated ventricular catheters. Can J Neurol Sci. 2004; 31(4):506–10. [PubMed: 15595257]

23. Kestle JR, Riva-Cambrin J, Wellons JC 3rd, Kulkarni AV, Whitehead WE, Walker ML, et al. A standardized protocol to reduce cerebrospinal fluid shunt infection: the Hydrocephalus Clinical Research Network Quality Improvement Initiative. J Neurosurg Pediatr. 2011; 8(1):22–9. [PubMed: 21721884]

24. Harris, CA., editor. The cellular and tissue response affecting catheters used in the treatment of hydrocephalus. Seventh meeting of the International Society for Hydrocephalus and CSF Disorders; 2015; Canada. 2015.

25. Lim, OWaL. Hydrophilic gels for biological use. Nature. 1960; 185:117–18.

26. Ferreira L, Vidal MM, Gil MH. Evaluation of poly(2-hydroxyethyl methacrylate) gels as drug delivery systems at different pH values. Int J Pharm. 2000; 194(2):169–80. [PubMed: 10692641]

27. Lu S, Anseth KS. Photopolymerization of multilaminated poly(HEMA) hydrogels for controlled release. J Control Release. 1999; 57(3):291–300. [PubMed: 9895416]

28. Nicolson PC, Vogt J. Soft contact lens polymers: an evolution. Biomaterials. 2001; 22(24):3273–83. [PubMed: 11700799]

29. Buwalda SJ, Boere KW, Dijkstra PJ, Feijen J, Vermonden T, Hennink WE. Hydrogels in a historical perspective: from simple networks to smart materials. J Control Release. 2014; 190:254–73. [PubMed: 24746623]

30. Song J, Saiz E, Bertozzi CR. A new approach to mineralization of biocompatible hydrogel scaffolds: an efficient process toward 3-dimensional bonelike composites. J Am Chem Soc. 2003; 125(5):1236–43. [PubMed: 12553825]

31. Filmon R, Grizon F, Basle MF, Chappaard D. Effects of negatively charged groups (carboxymethyl) on the calcification of poly(2-hydroxyethyl methacrylate). Biomaterials. 2002; 23(14):3053–9. [PubMed: 12069348]

32. Jhaveri SJ, Hynd MR, Dowell-Mesfin N, Turner JN, Shain W, Ober CK. Release of nerve growth factor from HEMA hydrogel-coated substrates and its effect on the differentiation of neural cells. Biomacromolecules. 2009; 10(1):174–83. [PubMed: 19061335]

33. Cook AD, Sagers RD, Pitt WG. Bacterial adhesion to poly(HEMA)-based hydrogels. J Biomed Mater Res. 1993; 27(1):119–26. [PubMed: 8420997]

34. Wong, TT., Liu, LL., Yeh, RS., Chang, SH., Ho, T., Niu, DM., Wang, GC., YJ. Hydrogel ventriculo-subdural shunt for the treatment of hydrocephalus in children. Springer; Japan: 1991.

35. Chan K, Gleason KK. Initiated chemical vapor deposition of linear and cross-linked poly(2-hydroxyethyl methacrylate) for use as thin-film hydrogels. Langmuir. 2005; 21(19):8930–9. [PubMed: 16142981]

36. Gleason, KK. CVD Polymers: Fabrication of Organic Surfaces and Devices. John Wiley & Sons; 2015.

37. Nejati S, Lau KK. Pore filling of nanostructured electrodes in dye sensitized solar cells by initiated chemical vapor deposition. Nano Lett. 2011; 11(2):419–23. [PubMed: 21171604]

38. Barr MC, Rowehl JA, Lunt RR, Xu J, Wang A, Boyce CM, et al. Direct monolithic integration of organic photovoltaic circuits on unmodified paper. Adv Mater. 2011; 23(31):3499–505. [PubMed: 21739489]

39. Park H, Howden RM, Barr MC, Bulovic V, Gleason K, Kong J. Organic solar cells with graphene electrodes and vapor printed poly(3,4-ethylenedioxythiophene) as the hole transporting layers. ACS Nano. 2012; 6(7):6370–7. [PubMed: 22724887]

40. Lau KKBJ, Teo KB, Chhowalla M, Amaratunga GA, Milne WI, McKinley GH, Gleason KK. Superhydrophobic carbon nanotube forests. nano letters. 2003; 3(12):1701–05.

41. Laird ED, Bose RK, Wang W, Lau KK, Li CY. Carbon nanotube-directed polytetrafluoroethylene crystal growth via initiated chemical vapor deposition. Macromol Rapid Commun. 2013; 34(3):251–6. [PubMed: 23225149]

42. Olceroglu E, Hsieh CY, Rahman MM, Lau KK, McCarthy M. Full-field dynamic characterization of superhydrophobic condensation on biotemplated nanostructured surfaces. Langmuir. 2014; 30(25):7556–66. [PubMed: 24882117]

43. Sojoudi H, Wang M, Boscher ND, McKinley GH, Gleason KK. Durable and scalable icephobic surfaces: similarities and distinctions from superhydrophobic surfaces. Soft Matter. 2016; 12(7): 1938–63. [PubMed: 26757856]

44. Hsieh CY, LK. Growth of Polyglycidol in Porous TiO2 Nanoparticle Networks via Initiated Chemical Vapor Deposition: Probing Polymer Confinement Under High Nanoparticle Loading. Advanced Materials Interfaces. 2015; 2(17)

45. Yang R, Jang H, Stocker R, Gleason KK. Synergistic prevention of biofouling in seawater desalination by zwitterionic surfaces and low-level chlorination. Adv Mater. 2014; 26(11):1711–8. [PubMed: 24375685]

46. Frampton JP, Hynd MR, Vargun A, Roysam B, Shain W. An in vitro system for modeling brain reactive responses and changes in neuroprosthetic device impedance. Conf Proc IEEE Eng Med Biol Soc. 2009; 2009:7155–8. [PubMed: 19965268]

47. You JB, Min KI, Lee B, Kim DP, Im SG. A doubly cross-linked nano-adhesive for the reliable sealing of flexible microfluidic devices. Lab Chip. 2013; 13(7):1266–72. [PubMed: 23381132]

48. Ozaydin-Ince G, Dubach JM, Gleason KK, Clark HA. Microworm optode sensors limit particle diffusion to enable in vivo measurements. Proc Natl Acad Sci U S A. 2011; 108(7):2656–61. [PubMed: 21282619]

49. Ince GO, Armagan E, Erdogan H, Buyukserin F, Uzun L, Demirel G. One-dimensional surface-imprinted polymeric nanotubes for specific biorecognition by initiated chemical vapor deposition (iCVD). ACS Appl Mater Interfaces. 2013; 5(14):6447–52. [PubMed: 23806214]

50. Lau KK, Gleason KK. All-dry synthesis and coating of methacrylic acid copolymers for controlled release. Macromol Biosci. 2007; 7(4):429–34. [PubMed: 17429803]

51. McInnes SJ, Szili EJ, Al-Bataineh SA, Xu J, Alf ME, Gleason KK, et al. Combination of iCVD and porous silicon for the development of a controlled drug delivery system. ACS Appl Mater Interfaces. 2012; 4(7):3566–74. [PubMed: 22720638]

52. O'Shaughnessy WS, Murthy SK, Edell DJ, Gleason KK. Stable biopassive insulation synthesized by initiated chemical vapor deposition of poly(1,3,5-trivinyltrimethylcyclotrisiloxane). Biomacromolecules. 2007; 8(8):2564–70. [PubMed: 17591748]

53. Bose RKNS, Stufflet DR, Lau KK. Graft polymerization of anti-fouling PEO surfaces by liquid-free initiated chemical vapor deposition. Macromolecules. 2012; 45(17):6915–22.

54. Yang RAA, Gleason KK. Design of conformal, substrate-independent surface modification for controlled protein adsorption by chemical vapor deposition (CVD). Soft Matter. 2012; 8(1):31–43.

55. Martin TP, Kooi SE, Chang SH, Sedransk KL, Gleason KK. Initiated chemical vapor deposition of antimicrobial polymer coatings. Biomaterials. 2007; 28(6):909–15. [PubMed: 17095086]

56. DiTizio V, Ferguson GW, Mittelman MW, Khoury AE, Bruce AW, DiCosmo F. A liposomal hydrogel for the prevention of bacterial adhesion to catheters. Biomaterials. 1998; 19(20):1877–84. [PubMed: 9855189]

57. Bose RK, Lau KK. Mechanical properties of ultrahigh molecular weight PHEMA hydrogels synthesized using initiated chemical vapor deposition. Biomacromolecules. 2010; 11(8):2116–22. [PubMed: 20690719]

58. Blasi E, Barluzzi R, Bocchini V, Mazzolla R, Bistoni F. Immortalization of murine microglial cells by a v-raf/v-myc carrying retrovirus. J Neuroimmunol. 1990; 27(2–3):229–37. [PubMed: 2110186]

59. Stansley B, Post J, Hensley K. A comparative review of cell culture systems for the study of microglial biology in Alzheimer's disease. J Neuroinflammation. 2012; 9:115. [PubMed: 22651808]

60. Rowley JA, Madlambayan G, Mooney DJ. Alginate hydrogels as synthetic extracellular matrix materials. Biomaterials. 1999; 20(1):45–53. [PubMed: 9916770]

61. Kuo CK, Ma PX. Ionically crosslinked alginate hydrogels as scaffolds for tissue engineering: part 1. Structure, gelation rate and mechanical properties. Biomaterials. 2001; 22(6):511–21. [PubMed: 11219714]

62. Frampton JP, Hynd MR, Williams JC, Shuler ML, Shain W. Three-dimensional hydrogel cultures for modeling changes in tissue impedance around microfabricated neural probes. J Neural Eng. 2007; 4(4):399–409. [PubMed: 18057507]

63. Frampton JP, Hynd MR, Shuler ML, Shain W. Fabrication and optimization of alginate hydrogel constructs for use in 3D neural cell culture. Biomed Mater. 2011; 6(1):015002. [PubMed: 21205998]

64. Nunamaker EA, Kipke DR. An alginate hydrogel dura mater replacement for use with intracortical electrodes. J Biomed Mater Res B Appl Biomater. 2010; 95(2):421–9. [PubMed: 20878928]

65. Gage GJ, Kipke DR, Shain W. Whole animal perfusion fixation for rodents. J Vis Exp. 2012; (65)

66. GO. Principles of polymerization. John Wiley & Son; 2004.

67. Beamson, GBD. High resolution XPS of organic polymers. Wiley; 1992.

68. Babar SLT, Abelson JR. Role of nucleation layer morphology in determining the statistical roughness of CVD-grown thin films. Journal of Vacuum Science & Technology A: Vacuum, Surfaces, and Films. 2014; 32(6):060601.

69. Babar SKN, Zhang P, Abelson JR, Dunbar AC, Daly SR, Girolami GS. Growth Inhibitor To Homogenize Nucleation and Obtain Smooth HfB2 Thin Films by Chemical Vapor Deposition. Chemistry of Materials. 2013; 25(5):662–7.

70. Craighead HGTS, Davis RC, James C, Perez AM, John PS, Isaacson MS, Kam L, Shain W, Turner JN, Banker G. Chemical and topographical surface modification for control of central nervous system cell adhesion. Biomedical Microdevices. 1998; 1(1):49–64.

71. Turner AM, Dowell N, Turner SW, Kam L, Isaacson M, Turner JN, et al. Attachment of astroglial cells to microfabricated pillar arrays of different geometries. J Biomed Mater Res. 2000; 51(3): 430–41. [PubMed: 10880086]

72. Minev IR, Moshayedi P, Fawcett JW, Lacour SP. Interaction of glia with a compliant, microstructured silicone surface. Acta Biomater. 2013; 9(6):6936–42. [PubMed: 23499849]

73. Janakiraman SFS, Hsieh CY, Smolin YY, Soroush M, Lau KK. Kinetic analysis of the initiated chemical vapor deposition of poly (vinylpyrrolidone) and poly (4-vinylpyridine). Thin Solid Films. 2015; 595:244–50.
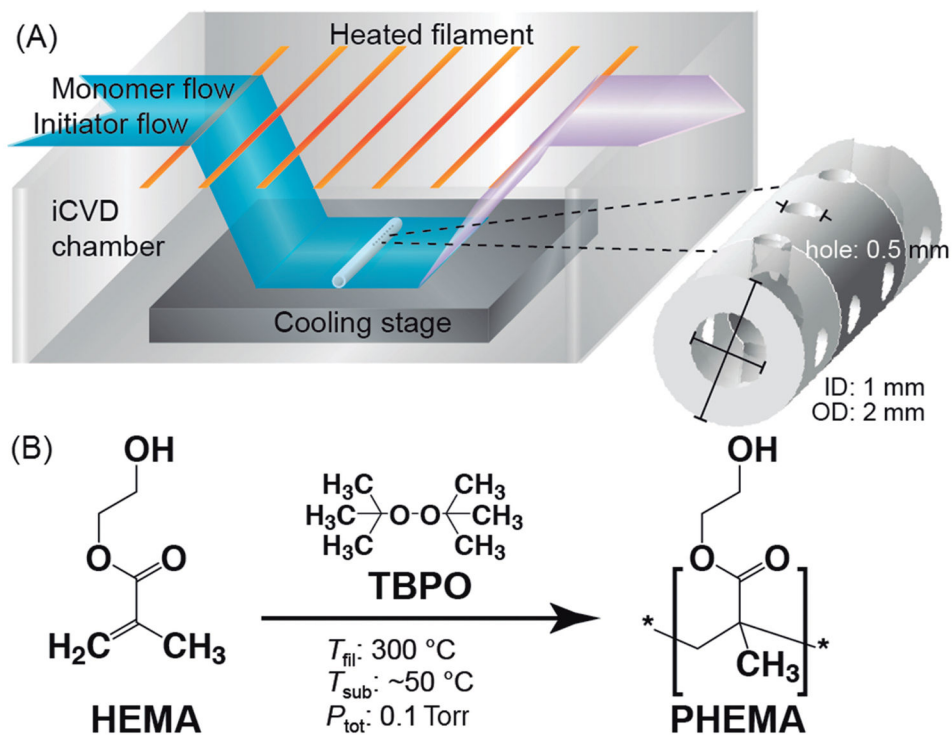
Fig. 1. iCVD polymerization and coating of PHEMA on PDMS ventricular catheters
(A) iCVD scheme for coating of PHEMA on the catheters. Each catheter has an outer and inner diameter of 2 and 1 mm, respectively. There are a series of intake holes, 0.5 mm in diameter, near the blind end that are arranged as eight holes spaced 1 mm apart in four rows at 90° apart around the tube circumference. (B) Free radical polymerization reaction to form PHEMA using HEMA monomer and TBPO initiator. With the cooling stage and heated filaments at 25 and 300 °C, respectively, and the reactor pressure at 0.1 Torr, the actual temperature of the catheter surface was recorded to be ≈50 °C.
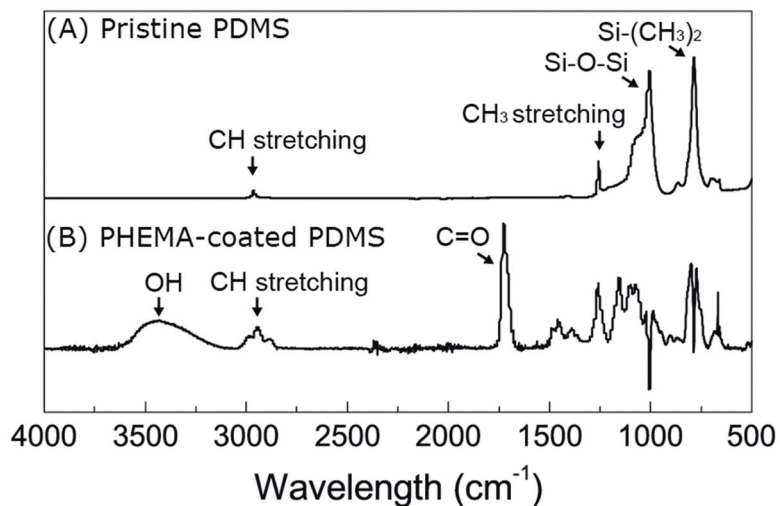
Fig. 2. Qualitative spectroscopic analysis of uncoated and PHEMA-coated PDMS ventricular catheters

ATR-FTIR spectra of (A) pristine and (B) iCVD PHEMA-coated PDMS catheters. The PDMS background was subtracted out of the PHEMA-coated PDMS spectrum. The OH (3434 cm^{-1}) and C=O (1726 cm^{-1}) peaks of PHEMA suggest that PHEMA was successfully deposited on the catheters.
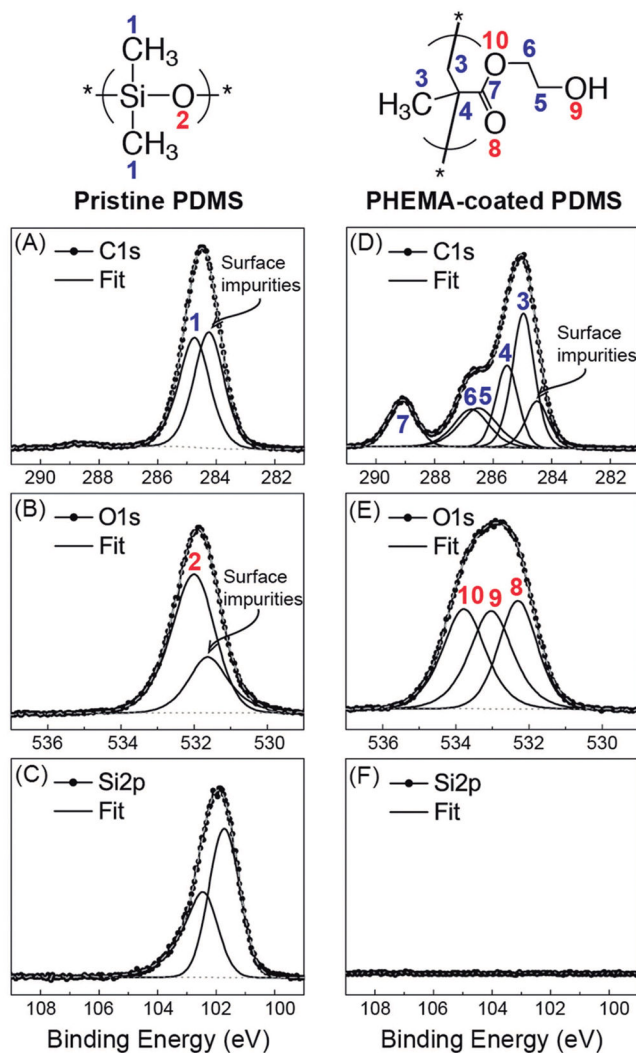
Fig. 3. Quantitative spectroscopic analysis of uncoated and PHEMA-coated PDMS ventricular catheters

High resolution C1s, O1s, and Si2p XPS spectra of pristine (A–C) and iCVD PHEMA-coated (D–F) PDMS catheters with their corresponding fitted peaks and peak assignments (see Table 1 also). The C:O:Si ratio of pristine PDMS, estimated at 2.1:1.0:1.0, agrees well with stoichiometric PDMS. The C:O ratio of the PHEMA coating, estimated at 2.5:1.0, is close to that of stoichiometric PHEMA. The disappearance of Si in the PHEMA-coated sample indicates the PHEMA coating is sufficiently thick to prevent the underlying PDMS substrate from being probed.
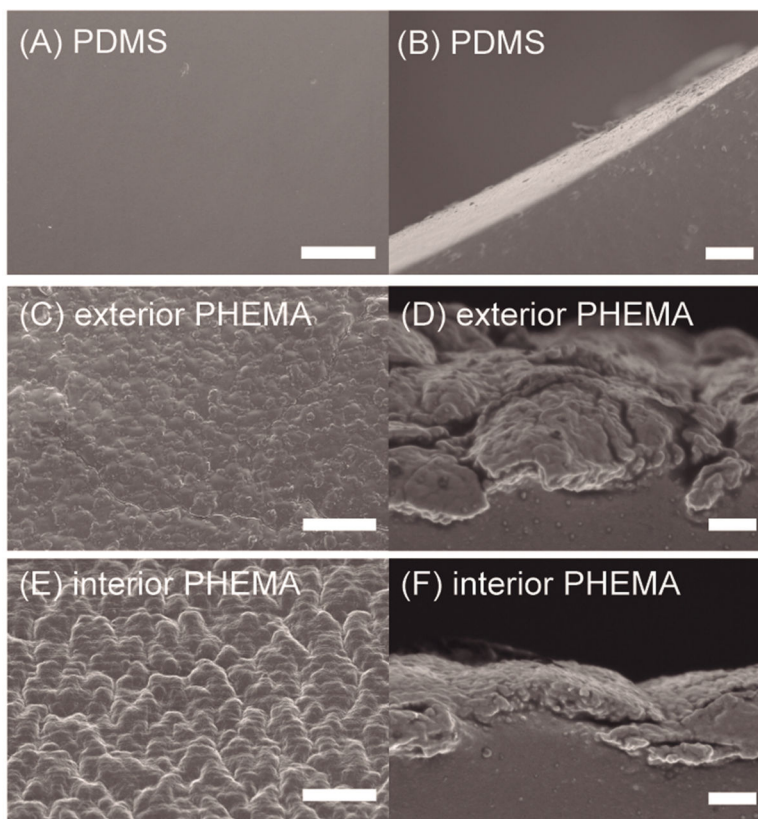
Fig. 4. Surface morphological analysis of uncoated and PHEMA-coated ventricular catheters
Top- and side-view SEM images of pristine (A,B) and iCVD PHEMA-coated (C,D and E,F)
PDMS catheters. The latter pairs of images are for PHEMA coatings on the exterior (C,D)
and interior (E,F) catheter walls, respectively. Surface roughness and feature sizes are related
to the nucleation density for polymer growth that is affected by the accessibility of activated
initiator species. Scale bar is 10 and 1 μm for top and side views, respectively.
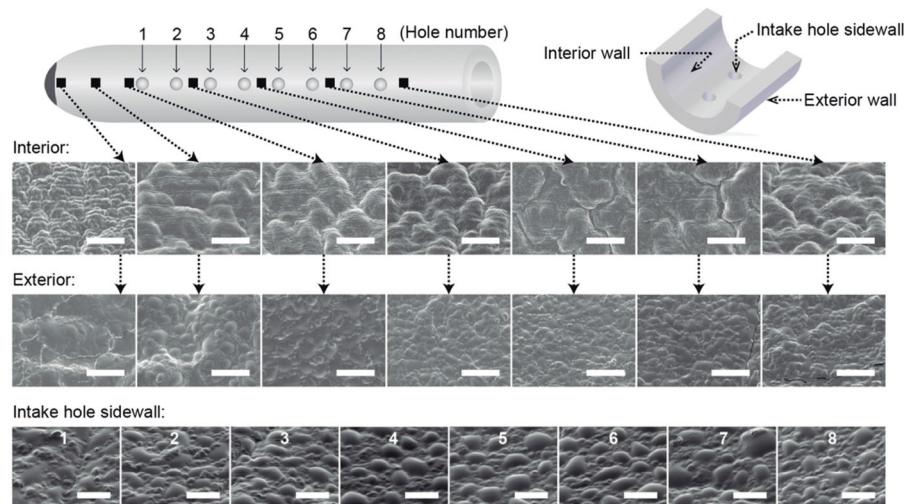
Fig. 5. PHEMA coating morphology along the PHEMA-coated ventricular catheters
Top view SEM images at different locations along the axial direction of the catheter of the PHEMA coating on the exterior and interior walls (identified by ν) as well as on the intake hole sidewalls (numbered 1–8) along a row of 8 intake holes. Surface roughness and feature sizes appear to be similar at various locations along the catheter indicating the highly uniform nature of the iCVD process. Differences in morphology on the exterior/interior/ intake hole walls as well as near the blind end are due to differences in activated initiator availability and nucleation density. Scale bar is 5 and 2.5 μm for interior/exterior and intake hole surfaces, respectively.
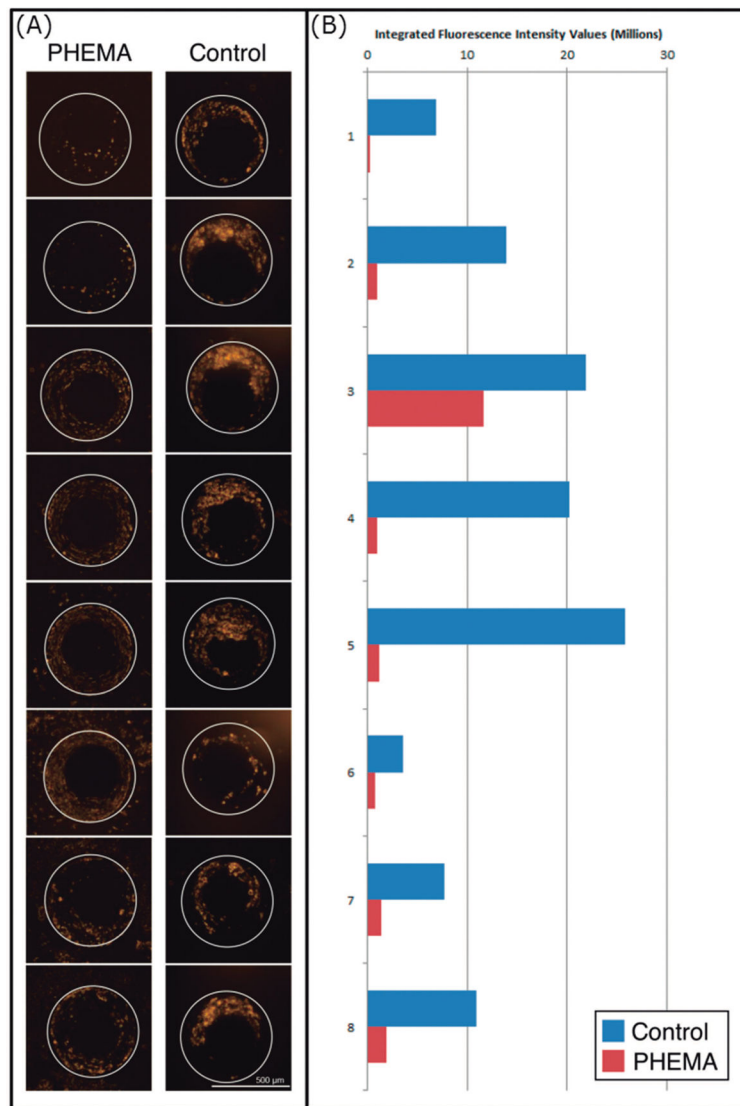
Fig. 6. Representative rhodamine-phalloid actin stain imaging for control and PHEMA CSF intake holes alongside calculated integrated fluorescence intensity values

(A) Eight representative CSF intake hole maximum projection images from the PHEMA coated and uncoated control catheter are shown at the 17-day time point. (B) The measured integrated fluorescence intensity values for the holes imaged are shown graphically. The CSF intake holes imaged are numbered one through eight, with hole one being closest to the catheter tip (most distal) and hole eight being closest to the alginate matrix loaded with cultured astrocytes and microglia (most proximal).

Table 1

Position and percent area of fitted peaks in high resolution XPS spectra

Core Level Electrons	Peak Number	Bonding Environment	Binding Energy (eV)	Area (atomic %)
		PDMS ventricular catheter		
C1s	–	Carbon impurities	284.2	32.7
	1	C*–Si	284.7	31.5
O1s	–	Oxygen impurities	531.6	5.8
	2	Si–O*	532.0	14.9
Si2p	–	Si2p$_{3/2}$	101.6	10.1
	–	Si2p$_{1/2}$	102.3	5.0
		PHEMA-coated catheter		
C1s	–	Carbon impurities	284.2	4.1
	3	–C*H$_2$–C(C*H$_3$)–	285.1	21.3
	4	–CH$_2$–C*(CH$_3$)–	285.7	11.0
	5	O–C–C*–OH	286.5	10.8
	6	O–C*–C–OH	287.0	10.8
	7	O–C*=O	289.1	10.5
O1s	8	O–C=O*	532.5	10.5
	9	O–C–C–O*H	533.2	10.5
	10	O*–C–C–OH	533.9	10.5